Display of Phosphorus-Containing Components on Low-Frequency Magnetic Resonance Images Using Double Magnetic Resonance

Sergey Shubin, Viatcheslav Frolov & Konstantin Tyutyukin

Applied Magnetic Resonance

ISSN 0937-9347

Appl Magn Reson
DOI 10.1007/s00723-019-01174-0

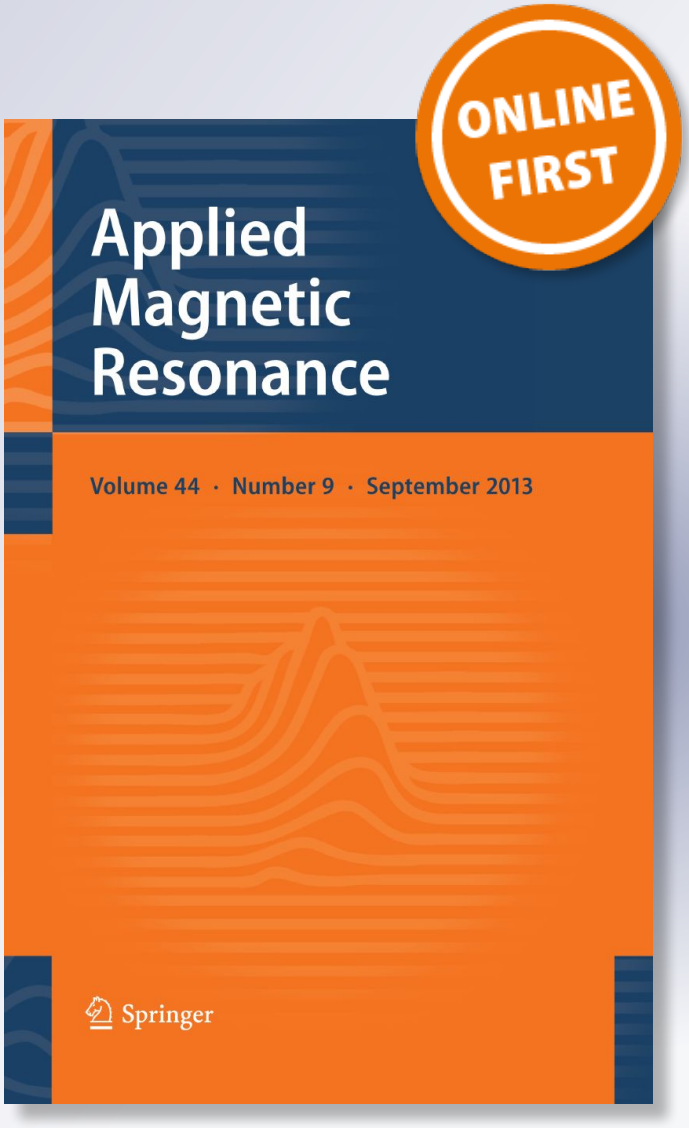

Springer

Applied Magnetic Resonance
https://doi.org/10.1007/s00723-019-01174-0

Applied
Magnetic Resonance

ORIGINAL PAPER

Display of Phosphorus-Containing Components on Low-Frequency Magnetic Resonance Images Using Double Magnetic Resonance

Sergey Shubin[1] · Viatcheslav Frolov[1] · Konstantin Tyutyukin[1]

Received: 27 July 2019 / Revised: 1 November 2019

Abstract
One of the promising areas in MRI diagnostics is the mapping of the distribution of nuclei other than ^{1}H. It is caused by the presence of such nuclei in molecules involved in important biological processes. The spatial distribution of these nuclei in a body can be judged on those or other pathological processes occurring in it. One of such nuclei is ^{31}P, which plays an important role in a living organism. So, adenosine triphosphate is a main metabolite that plays a fundamental role as an energy transfer molecule and is involved in the construction of the cell membrane and in many other processes, for example, a phosphate donor and a signaling molecule inside the cells. This work presents the technique of displaying phosphorus-containing components in a ultralow magnetic field (7 mT) without a receiving signal of ^{31}P using the double magnetic resonance method. The working substance in a phantom was the compound trimethyl phosphate $(CH_3O)_3PO$.

1 Introduction

Current trends in the development of magnetic resonance imaging (MRI) go beyond the classic experiment displaying the distribution of ^{1}H in a body [1–3]. For more diagnostic information, technologies of visualization of various physical parameters are being developed [4], and this paper describes one of such approaches.

In the described experiment an obtaining MRI of the spatial distribution of phosphorus in an object to study is based on the double resonance spin echo (DRSE) technique [5–7]. When the 90-τ-180-τ-echo pulse sequence acts on protons, during the action of the 180° pulse at the hydrogen frequency, the 180° pulse is sent at the phosphorus (^{31}P) frequency. An RF pulse sequence is applied to the ^{1}H–^{31}P two-spin system with the scalar spin–spin coupling. The application

✉ Viatcheslav Frolov
vfrolovv@bk.ru

[1] St. Petersburg State University, 1, Ulyanovskaya Str., Saint Petersburg 198504, Russian Federation

Published online: 02 December 2019

of this method allows obtaining an MRI of the distribution of phosphorus with a sensitivity 16 times greater than the direct method. This is because the image is obtained indirectly as the difference of MRI received from all protons (without 180° pulse at the phosphorus frequency) and at presence of such pulse. As a result, we obtain an MR image of ^{1}H nuclei associated with ^{31}P nuclei, which is identical to the distribution of ^{31}P nuclei. This is especially important in the case of a weak field, where the problem of sensitivity is very acute. On the other hand, it is in a weak field that the internuclear scalar interactions manifest themselves most strongly, since the splittings caused by them do not depend on the field level.

In this paper, we present the theory of the method and its experimental realization using a phantom with trimethyl phosphate (TMP) $(CH_3O)_3PO$ in a magnetic field 7 mT.

2 Equipment

The experiment was carried out with a homebuilt magnetic resonance imager in a magnetic field 7 mT [8] complemented with a transmitting channel at NMR frequency of phosphorus nuclei ^{31}P. The above-mentioned channel consists

- A high-frequency generator at the NMR frequency of ^{31}P 125 kHz.
- Power amplifier at this frequency [9].
- Dual frequency sensor.
- Electronic control software.

In this work, a phantom containing water and TMP was used. The phantom was a two-section glass cylindrical flask (Fig. 1). The internal section is filled with TMP, while the external section is filled with water.

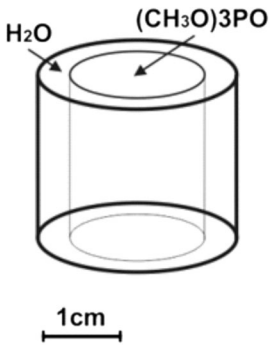

Fig. 1 Phantom water–trimethyl phosphate

3 Theoretical Calculation

The initial state of the two-spin system *H–P* (equilibrium state), in the presence of a constant magnetic field B_0 applied in the z direction, is described by the reduced density operator. The density operator is written as a combination of the identity matrix and the matrix of the operator I_z [10]:

$$\rho_0 = \begin{pmatrix} \frac{n}{2} + \Delta & 0 \\ 0 & \frac{n}{2} - \Delta \end{pmatrix} = \frac{n}{2}\begin{pmatrix} 1 & 0 \\ 0 & 1 \end{pmatrix} + 2\Delta\begin{pmatrix} \frac{1}{2} & 0 \\ 0 & -\frac{1}{2} \end{pmatrix} = \frac{n}{2}E + 2\Delta \cdot I_z, \tag{1}$$

$$E = \begin{pmatrix} 1 & 0 \\ 0 & 1 \end{pmatrix}, \tag{2}$$

$$\rho_0 = I_z + S_z, \tag{3}$$

where I_z is the projection operator of spin H onto the z axis, S_z is the projection operator of spin P onto the z axis, n is the number of molecules per unit volume, and Δ is the difference in population levels.

The Hamiltonian of the indirect spin–spin interaction takes the following form [11]:

$$H_J = 2\pi J S_z I_z. \tag{4}$$

The total Hamiltonian in the rotating frame, taking into account the chemical shift, can be written as follows:

$$H_{\text{full}} = 2\pi J S_z I_z + \omega_{\text{cs}} I_z, \tag{5}$$

where $\omega_{\text{cs}} I_z$ is the proton chemical shift Hamiltonian.

As a result of the action of 90° pulses on ^{1}H spins, the density matrix takes the following form:

$$\rho_1 = \mathrm{e}^{-iH_{\text{rf}}t_{90}}\rho_0\mathrm{e}^{iH_{\text{rf}}t_{90}} = I_x + S_z, \tag{6}$$

where $H_{\text{rf}} = B_1\gamma I_y$ is the Hamiltonian of the rf interaction and t_{90} is the length of the 90° pulse.

To calculate the resulting signal, we use the average Hamiltonian theory [10]. For this purpose, we calculate the effective Hamiltonian in a frame of reference associated with the RF interaction before and after the 180° pulse.

Let us consider the effect of a 180° pulse on ^{1}H and a pulse of arbitrary duration on ^{31}P on the total Hamiltonian of the internal spin–spin interactions.

The effective Hamiltonian of the system before applying the two pulses is

$$H_{\text{full}} = 2\pi J S_z I_z + \omega_{\text{cs}} I_z. \tag{7}$$

In the tilted frame, which is associated with the RF interaction, the Hamiltonian of the RF interactions can be written as follows:

$$H_{\mathrm{rf}} = \omega_{1I} I_x + \omega_{1S} S_x, \tag{8}$$

where we assume that $\omega_{1I} I_x$ and $\omega_{1S} S_x$ are much larger than all the internal interactions in the Hamiltonian H_{full}. Thus, during the RF irradiation, the internal interactions are ignored.

Upon the transfer to the reference frame associated with the RF interaction, the internal Hamiltonian $\tilde{H}_{\mathrm{int}}$ in the new interaction frame is calculated in accordance with the expression:

$$\tilde{H}_{\mathrm{int}} = U^{\dagger}_{\mathrm{ext}}(t) H_{\mathrm{int}} U_{\mathrm{ext}}(t) - i U^{\dagger}_{\mathrm{ext}}(t) \frac{\mathrm{d}}{\mathrm{d}t} U_{\mathrm{ext}}(t), \tag{9}$$

where $U_{\mathrm{ext}}(t) = \mathrm{e}^{-iH_{\mathrm{rf}} t_{\mathrm{p}}}$ is the propagator of the RF interaction H_{rf} and t_{p} is the length of the RF pulse.

$\tilde{H}_{\mathrm{full2}} = U^{\dagger}_{\mathrm{ext}} H_{\mathrm{full}} U_{\mathrm{ext}}$ is the Hamiltonian of the system after the 180° and X° pulses:

$$\begin{aligned} \tilde{H}_{\mathrm{full2}} &= \mathrm{e}^{iH_{\mathrm{rf}} t_{\mathrm{p}}} (\omega(r) I_z + 2\pi J S_z I_z + \omega_{\mathrm{cs}} I_z) \mathrm{e}^{-iH_{\mathrm{rf}} t_{\mathrm{p}}} \\ &= \mathrm{e}^{iH_{\mathrm{rf}} t_{\mathrm{p}}} (\omega(r) I_z + \omega_{\mathrm{cs}} I_z) \mathrm{e}^{-iH_{\mathrm{rf}} t_{\mathrm{p}}} + \mathrm{e}^{iH_{\mathrm{rf}} t_{\mathrm{p}}} (2\pi J S_z I_z) \mathrm{e}^{-iH_{\mathrm{rf}} t_{\mathrm{p}}}. \end{aligned} \tag{10}$$

Consider the two terms individually.

The first term after substitution of H_{int} becomes:

$$\tilde{H}^{(1)}_{\mathrm{full2}} = \mathrm{e}^{iH_{\mathrm{rf}} t_{\mathrm{p}}} (\omega(r) I_z + \omega_{\mathrm{cs}} I_z) \mathrm{e}^{-iH_{\mathrm{rf}} t_{\mathrm{p}}}. \tag{11}$$

$H_{\mathrm{rf}} = \omega_{1I} I_x + \omega_{1S} S_x$—since RF interactions, applied to nuclei of different types, do not affect each other or, in other words, the corresponding operators I_x and S_x commute, the effect of the two pulses can be considered separately. Therefore, the exponential operator in the expression can be divided into the product of two exponential operators. Therefore, to analyze the influence of a 180° pulse on the chemical shift Hamiltonian and the inhomogeneity of the field, we can confine ourselves to that part of the preceding equation that contains the operators of the hydrogen nuclei:

$$\begin{aligned} \tilde{H}^{(1)}_{\mathrm{full2}} &= \mathrm{e}^{iH_{\mathrm{rf}} t_{\mathrm{p}}} (\omega(r) I_z + \omega_{\mathrm{cs}} I_z) \mathrm{e}^{-iH_{\mathrm{rf}} t_{\mathrm{p}}} = \mathrm{e}^{i\pi I_x} (\omega(r) I_z + \omega_{\mathrm{cs}} I_z) \mathrm{e}^{-i\pi I_x} \\ &= \mathrm{e}^{i\pi I_x} I_z \mathrm{e}^{-i\pi I_x} (\omega(r) + \omega_{\mathrm{cs}}) \\ &= (I_z \cos(\pi) + I_y \sin(\pi))(\omega(r) + \omega_{\mathrm{cs}}) \\ &= -(\omega(r) I_z + \omega_{cs} I_z). \end{aligned} \tag{12}$$

Thus, after the 180° pulses on protons, parts of the Hamiltonian linear in I_z change sign to the opposite.

Let us consider the second term in Eq. (10):

Since both terms in $H_{\mathrm{rf}} = \omega_{1I} I_x + \omega_{1S} S_x$ commute with each other, then

$$\begin{aligned}\tilde{H}^{(2)}_{\text{full2}} &= \mathrm{e}^{iH_{\text{rf}}t_{\text{p}}}(2\pi JS_zI_z)\mathrm{e}^{-iH_{\text{rf}}t_{\text{p}}} \\ &= \mathrm{e}^{i\omega_{1S}t_{\text{p}}S_x}(2\pi JS_zI_z)\mathrm{e}^{-i\pi I_x}\mathrm{e}^{-i\omega_{1S}t_{\text{p}}S_x} \\ &= 2\pi J\mathrm{e}^{i\pi I_x}(I_z)\mathrm{e}^{-i\pi I_x}\mathrm{e}^{i\omega_{1S}t_{\text{p}}S_x}(S_z)\mathrm{e}^{-i\omega_{1S}t_{\text{p}}S_x},\end{aligned} \tag{13}$$

$$\tilde{H}^{(2)}_{\text{full2}} = 2\pi J(I_z\cos(\pi) + I_y\sin(\pi))(S_z\cos(\omega_{1S}t_{\text{p}}) + S_y\sin(\omega_{1S}t_{\text{p}})). \tag{14}$$

If the rotation angles of the pulses in both channels are equal to 180° in the experiment, then the Hamiltonian does not change. Then throughout the entire experiment, the effective (average) spin Hamiltonian is equal:

$$\tilde{H} = \frac{(H_{\text{full}}\tau + \tilde{H}_{\text{full2}}\tau)}{2\tau}, \tag{15}$$

$$\bar{H} = \frac{2\pi JS_zI_z\tau - 2\pi JI_z(S_z\cos\omega_{1S}t_{\text{p}} + S_y\sin\omega_{1S}t_{\text{p}})\tau}{2\tau}, \tag{16}$$

$$\bar{H} = \pi J[S_zI_z - I_z(S_z\cos\omega_{1S}t_{\text{p}} + S_y\sin\omega_{1S}t_{\text{p}})], \tag{17}$$

$$\tilde{H}_{\text{full2}} = -(\omega(r)I_z + \omega_{\text{cs}}I_z) + 2\pi JI_z\cos(\pi) + I_y\sin(\pi))(S_z\cos(\omega_{1S}t_{\text{p}}) + S_y\sin(\omega_{1S}t_{\text{p}})), \tag{18}$$

$$\tilde{H}_{\text{full2}} = -(\omega(r)I_z + \omega_{\text{cs}}I_z) + 2\pi J(-I_z)(S_z\cos(\omega_{1S}t_{\text{p}}) + S_y\sin(\omega_{1S}t_{\text{p}})). \tag{19}$$

In the case of 180° pulses, the last expression equals to $2\pi JS_zI_z$.

Thus, as a result of the action of this pulse sequence, the chemical shifts and inhomogeneity of the static magnetic field B_0 are averaged (spin echo), while the effective average Hamiltonian of the spin–spin interactions does not equal to zero in general.

Let us consider the effect of the average Hamiltonian on the density matrix:

$$\rho_1 = I_x + S_z - \text{density matrix after a } 90^\circ \text{ pulse},$$

$$\rho_2 = U_{\text{evol}}\rho_1U^{\dagger}_{\text{evol}}, \tag{20}$$

$$U_{\text{evol}} = \mathrm{e}^{-i\bar{H}t}, \tag{21}$$

$$\rho_2 = \mathrm{e}^{-i2\pi JI_zS_z2\tau}\rho_1\mathrm{e}^{i2\pi JI_zS_z2\tau}. \tag{22}$$

Let us consider the effect of the Hamiltonian on the hydrogen part of the density matrix. In this case, the term of the density matrix describing the state of the phosphorus nuclei, S_z, is excluded from consideration, since the operator S_z commutes with the average spin Hamiltonian ($[S_z, 2I_zS_z]=0$). Consequently, the orientation of the spins of the phosphorus nuclei does not change.

Since there are three operators for which the cyclic commutation relation is fulfilled: $I_x, 2I_yS_z, 2I_zS_z$, we can write:

$$\rho_{\text{final}} = \mathrm{e}^{-i\pi J 2I_zS_z 2\tau} I_x \mathrm{e}^{i\pi J 2I_zS_z 2\tau}, \tag{23}$$

$$\rho_{\text{final}} = I_x(\cos(2\pi J\tau) + 2I_yS_z \sin(2\pi J\tau)). \tag{24}$$

The observed signal can be calculated according to the following equation [10]:

$$S(t) = Tr\{(I_x(\cos(2\pi J\tau) + 2I_yS_z \sin(2\pi J\tau)))(I_x + iI_y)\}. \tag{25}$$

As only the first term is directly detected in the experiment, the following condition must be fulfilled for minimization of the observed signal: $2\pi J\tau = \frac{\pi}{2}$, which leads to $\tau = \frac{1}{4J}$. In this case, one achieves the maximal contrast between different parts of the sample, where coupled and non-coupled subsystems are localized. The echo signal detected by the receiving RF coil from the J-coupled spins is absent in this case.

Figure 2 presents the theoretical dependence of the echo amplitude on τ.

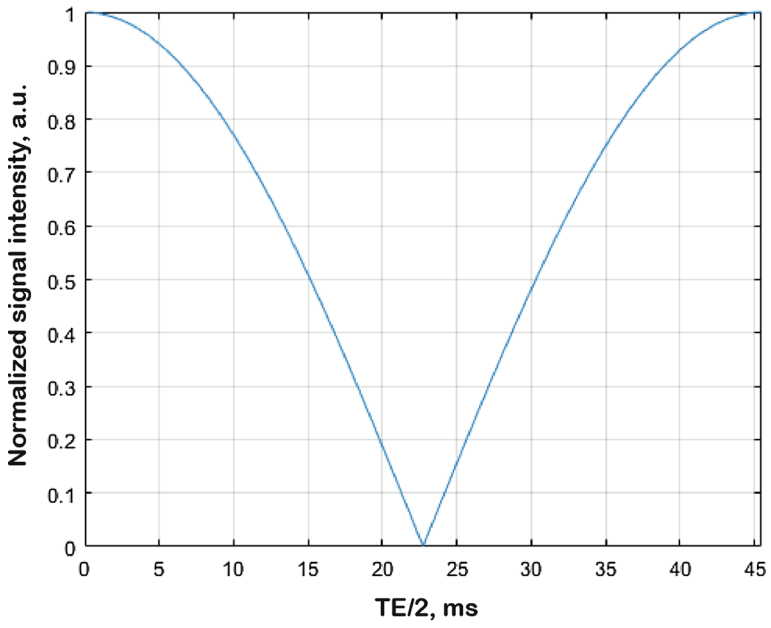

Fig. 2 Theoretical dependence of the proton echo amplitude on τ on condition of action of 180° ^{31}P pulse

4 Experimental Results

To check the result of the above described experiment, we obtained a series of MR images with suppression of proton signal from the ^{31}P-containing component. Figure 3 shows the pairs of pictures that were obtained with different extents of impact that inverting ^{31}P pulse made on the system. The left images in the depicted series were received with the switched-off inverting ^{31}P pulse, i.e., we obtained an image of the full distribution of protons on the sample. The right images were recorded with the switched-on phosphorus inverting pulse. The series demonstrate how the suppression depends on the echo delay parameter τ. It is seen that the maximum effect is obtained when $\tau = 22.5$ ms, which corresponds to that calculated from the ^{31}P–^{1}H J-coupling constant (11 Hz) theoretical value.

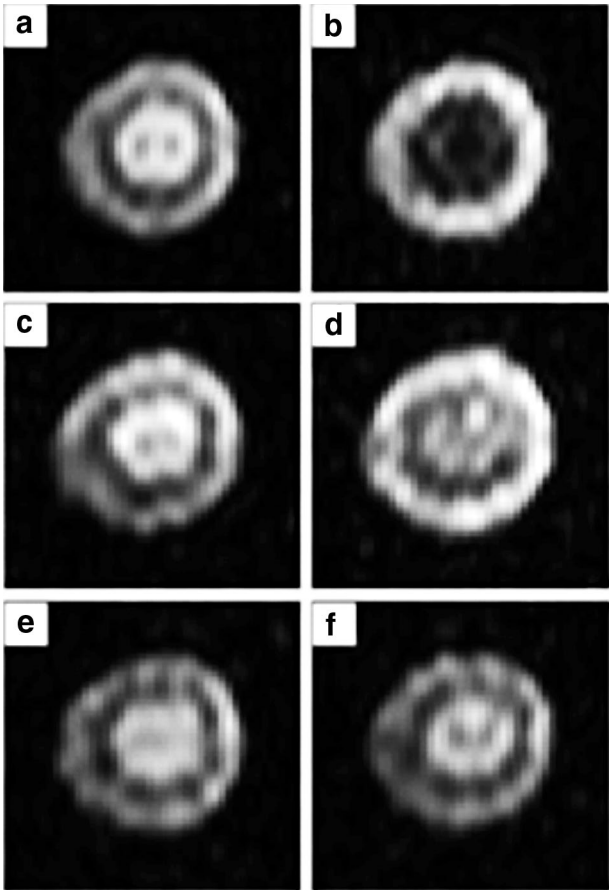

Fig. 3 Proton MR images of the phantom with 180° ^{31}P pulse on or off and by various values of τ: **a** rf pulse on ^{31}P channel is off, $\tau = 22.5$ ms, **b** ^{31}P rf pulse is on, $\tau = 22.5$ ms, **c** ^{31}P rf pulse is off, $\tau = 33.5$ ms, **d** ^{31}P rf pulse is on, $\tau = 33.5$ ms, **e** ^{31}P rf pulse is off, $\tau = 45$ ms, **f** ^{31}P rf pulse is on, $\tau = 45$ ms

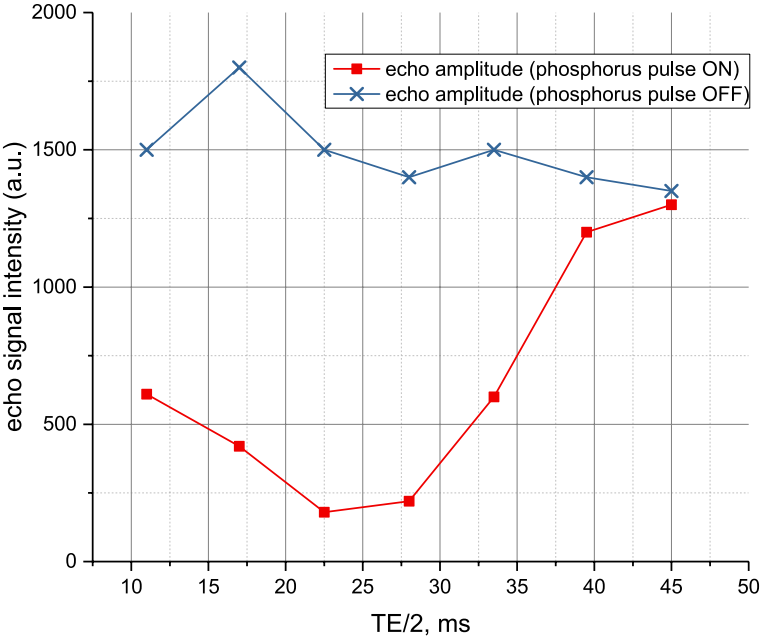

Fig. 4 Dependence of the experimental proton echo amplitudes on τ (τ=TE/2) for a case with lack of an impulse on phosphorus and a case with its existence

In Fig. 4, the experimental dependence of proton signal from TMP on τ is presented for the cases with the presence of phosphorus inverting pulse (upper graph) and its absence (lower graph). Figure 5 demonstrates the effect of proton signal suppression more visually.

5 Conclusion

The graphs presented in Figs. 2, 4 and 5 and MR images with signal suppression from ^{1}H associated with ^{31}P in Figs. 3 and 6 show that the obtained experimental data completely confirm the theoretical calculation. The maximum effect of suppression of the proton signal were observed at $\tau = (1/4)J$. Thus, the described method allowed visualizing a spatial distribution of phosphorus without direct observation of the phosphorus image that provided a sufficient sensitivity to carry out an experiment at ultralow magnetic field.

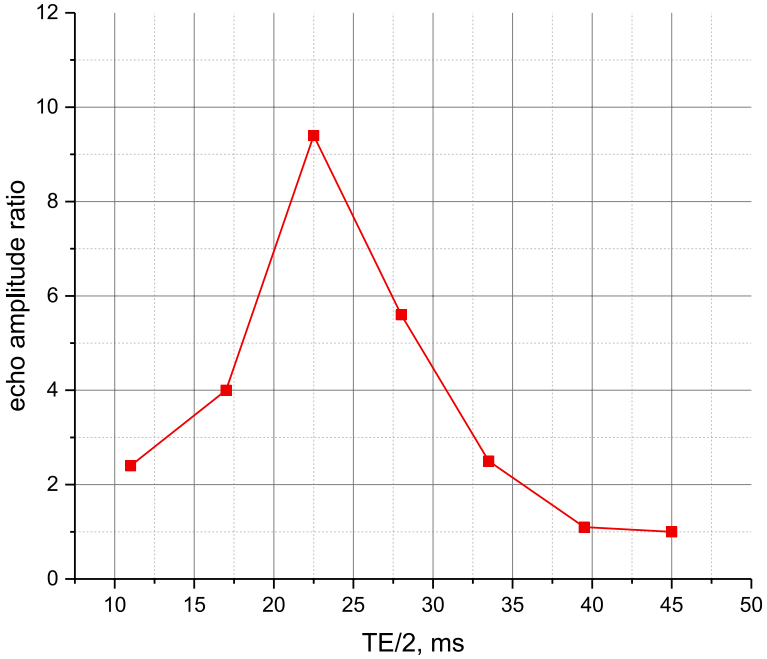

Fig. 5 Dependence of the ratio of the experimental proton echo amplitudes on τ ($\tau = \mathrm{TE}/2$), when the pulse on $^{31}\mathrm{P}$ is off and on

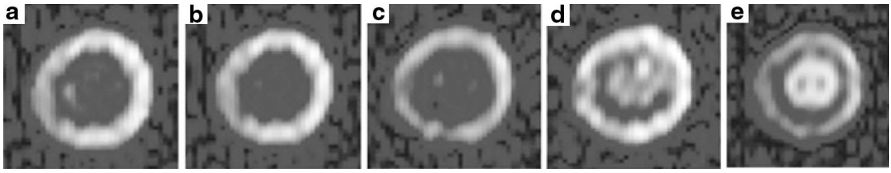

Fig. 6 MR images of the phantom with TMP proton signal suppression at various values of τ: **a** 17 ms, **b** 22.5 ms, **c** 28 ms, **d** 33.5 ms, **e** 45 ms

References

1. B.M. Dale, M.A. Brown, R.C. Semelka, *MRI: Basic Principles and Applications*, 3rd edn. (Wiley, New York, 2015), p. 234
2. P.A. Rinck, *Magnetic Resonance in Medicine* (Blackwell Wissenschafts, Berlin, 2001), p. 245
3. V. Kuperman, *Magnetic Resonance Imaging: Physical Principles and Applications* (Academic Press, San Diego, 2000), p. 182
4. S.V. Ievleva, N.V. Luzhetckaia, K.V. Tyutyukin, V.V. Frolov, Appl. Magn. Reson. **48**, 699–706 (2017)
5. R.R. Ernst, G. Bodenhausen, A. Wokaun, *Principles of Nuclear Magnetic Resonance in One and Two Dimensions* (Clarendon Press, Oxford, 1987), p. 710
6. G. Webb, S.C.R. Williams, L.D. Hall, J. Magn. Reson. **84**, 159–165 (1989)

7. L.D. Hall, T.J. Norwood, S.C.R. Williams, J. Magn. Reson. **79**(2), 363–368 (1988)
8. V. Frolov, in *Book of Abstracts of 2nd International Conference on Magnetic Resonance Microscopy* (Heidelberg, Germany, 6–9 September 1993), Paper MET-23
9. E.T. Red, *Arbeitsbuch fur den HF-Techniker* (Franzis-Verlag GmbH, Miinchen, 1986), p. 256
10. M.H. Levitt, *Spin Dynamics: Basics of Nuclear Magnetic Resonance*, 2nd edn. (Wiley, New York, 2008), p. 744
11. V.I. Chizhik, Y.S. Chernyshev, A.V. Donets, V.V. Frolov, A.V. Komolkin, M.G. Shelyapina, *Magnetic Resonance and Its Applications* (Springer, Berlin, 2014), p. 782